Moonlight Sonata: Unsupervised Denoising of Permanently Shadowed Lunar Regions with Filtered Diffusion Model

Alik Mondal
University of Delhi
Dwarka, New Delhi
edualik801@gmail.com

Rishitosh K. Sinha
Physical Research Laboratory
Ahmedabad, Gujrat
rishitosh@prl.res.in

Abstract

Permanently shadowed regions (PSRs) on the lunar pole contain clues about lunar geology and the presence of water-ice, but they are challenging to analyze due to extreme low-light imaging conditions. Recent advances in low-light image denoising are promising, but they either require an effective physical noise model or clean target images, and are not as effective in extreme imaging scenarios with limited and constrained data. We present an unsupervised denoising approach that recovers high-quality images from noisy, low-light data without requiring clean targets or noise models. Our approach trains a diffusion probabilistic model on well-lit lunar surface images obtained from the Orbiter High Resolution Camera onboard Chandrayaan-2's Orbiter to learn a qualitative prior. This enables and accelerates the denoising workflow. Despite differences in noise profiles across sensors, we further demonstrate cross-inferencing of images from the Narrow Angle Camera (NAC) onboard the Lunar Reconnaissance Orbiter. Our unsupervised framework significantly outperforms baseline methods and nearly matches state-of-the-art supervised techniques. It enables detailed analysis of extensive archives of lunar images to unlock insights into PSR composition, topology, ice detection, and rover planning where shadows obstruct direct observation. The ability to denoise with limited data makes our method promising for extreme imaging scenarios across robotic sensing applications.

1. Introduction (also name image stripe ID)

Structured sensor-related noise, such as photon noise, dark-current noise, and others, is very challenging to remove in a low-light setting. However, the absence of any literature regarding the noise distribution increases the difficulty tenfold. It is not possible to create an exact noise model for subtraction from the noisy image. Instead, we take an approach to approximate the noise profile. Therefore, unsupervised approaches can be highly effective in extreme imaging scenarios to improve image quality.

The traditional method for removing such noise sources involves extending the sensor exposure time, as done in CH2's OHRC with 128-256 time-delayed frame integration to address this issue. Additionally, Burst Photography is used to enhance image quality. However, all these traditional denoising methods struggle to capture the high-level features of an image.

In a supervised manner, learning-based denoising methods are employed, but they require an extensive collection of high-quality noisy-clean image pairs or a noise model, which isn't always readily available. Ultimately, any synthetic physical noise model may suffer from poor generalization issues. To mitigate this problem, self-supervised methods that attempt to identify and remove structured noise patterns have been developed. However, they often assume independence from pixel location.

Unsupervised approaches using architectural priors or informative priors for denoising are also commonly used but are limited by the representability of the dataset or the overall non-linear nature of the noise. In this work, we present a denoising approach for extreme low-light imaging scenarios, specifically those in Permanently Shadowed Regions (PSRs) on the lunar surface, as captured by Chandrayaan-2's Orbiter High Resolution Camera (OHRC). The OHRC dataset is limited, with very few sample stripes, and lacks defined information on the noise distribution. Thus, devising an unsupervised approach to enhance the quality of these images, in highly-constrained cases, could have significant scientific impact. For instance, it could aid in geological investigations of obscured regions, such as crater dating, reducing uncertainty in rover and human traverse planning. It can also be valuable in the search for polar ice-traps on the lunar poles. In this paper, we introduce a novel denoising workflow to eliminate the CCD sensor noise affecting the PSR images in an unsupervised manner, even with an extremely limited dataset. Firstly, we train a probabilistic diffusion model on sunlit lunar surfaces to obtain information about lunar surface statistics. We then use this information as a prior to accelerate lunar surface reconstruction relative to the sensor noise. Secondly, we introduce an acceleration unit to further expedite the

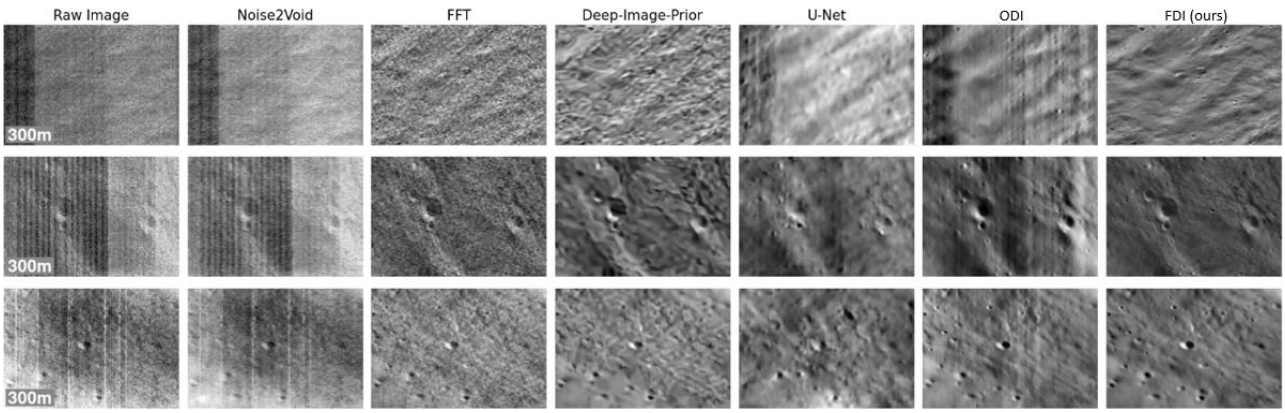

Figure 1: OHRC denoised image

surface reconstruction, utilizing frequency priors. During the denoising process, During the denoising process, we aim to simulate the noise formation in the noisy image and halt the process just before noise reconstruction begins. Finally, we employ this trained network to perform cross-inference for the Lunar Reconnaissance Orbiter's (LRO) Narrow Angle Camera. (NAC).

Our main contributions are summarized as follows:

- We have devised a novel unsupervised approach for low-light denoising in extreme scenarios for PSR images at the lunar poles.
- We have highlighted the cross-inferential nature of our model, capable of performing out-of-distribution inference on LRO's NAC images.
- The qualitative and quantitative results obtained from our approach strongly outperform the existing calibration baselines and other unsupervised denoising methods, nearly achieving the state-of-the-art performance in supervised denoising.

2. Related Work (DDRM?)

The enhancement and correction of noise in images of Permanently Shadowed Region (PSR) have been the subject of extensive research efforts. In the context of the Chandrayaan-2 OHRC image dataset, prior work primarily focused on calibration routines [x]. However, numerous approaches have been explored in the broader field of image denoising. These encompass spatial filtering [x], image prior-based methods [x], and traditional techniques such as histogram equalization and gamma correction [x]. In addition to these, advanced deep learning methods, including the U-Net architecture [x] and frequency domain conversion enhancement [x], have been proposed to address noise in low-illumination conditions.

Addressing the scarcity of usable image data, some researchers have adopted synthetic data generation techniques. These approaches involve models like Gaussian noise modeling [x], the integration of real and synthetic data in varying proportions [x], and denoising strategies tailored for extreme low-light conditions [x]. Generative methods, such as autoencoders, GANs [x], and pixel-wise generation [x], have also been explored for enhancing low-light images.

The domain of unsupervised denoising has yielded a rich and diverse literature, with notable contributions like Noise2Noise (N2V) [x] and Noise2Void (N2V) [x], which map corruption to corruption or do so without considering subsequent corruption, respectively. Convolutional Variational Autoencoders (VAE), with approaches like DivNoising [x] and its hierarchical latent space variant, HDN [x], have shown promise in generating plausible denoising solutions for complex inverse problems. Recent advancements have even tackled structured noises using similar implementations [x], marking the latest progress in this domain.

However, the state-of-the-art in PSR image denoising is exemplified by the HORUS method [x], which employs a supervised approach coupled with a physical noise model. It has demonstrated remarkable success in denoising and enhancing PSRs sampled from the LROC NAC raw dataset. Nevertheless, our research takes a different, completely unsupervised approach, distinct from traditional supervised methods, as it does not rely on training pairs or a physical noise model. Instead, it leverages extensive training on the Chandrayaan-2 OHRC image data, which offers a higher spatial resolution comparative to previous datasets.

3. Instrument overview

One of the payloads carried by the Chandrayaan-2 Orbiter is the Orbiter High-Resolution Camera (OHRC) (Fig. 2.1). With the mission goal of imaging the landing location before landing and the science goal of imaging small-scale features in fine detail close to the polar regions,

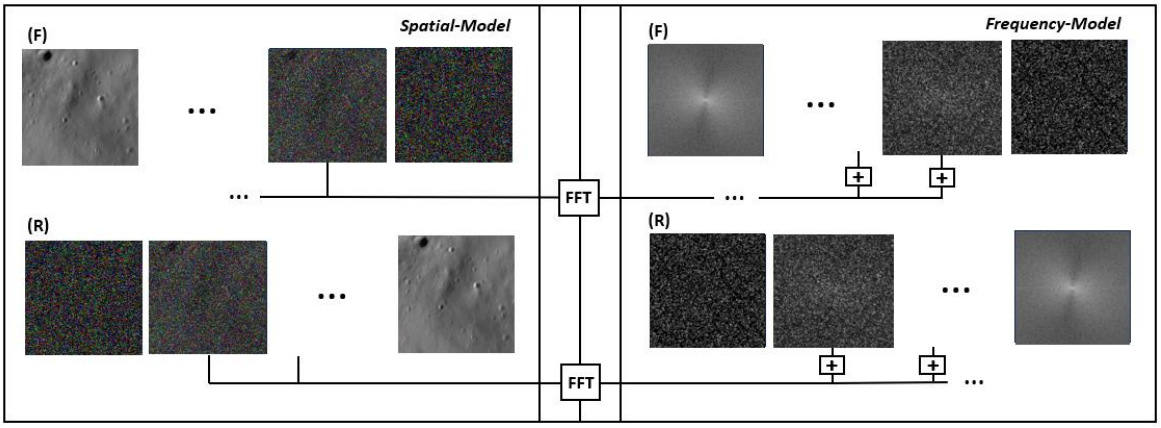

Figure 2: Training of Spatial and Frequency models for prior injection.

it is a very high-resolution camera that operates in the visible band. The ground sample distance (GSD) and sweep width of the Chandrayaan-2 OHRC (Orbiter High-Resolution Camera) are 0.25 m and 3 km, respectively, from an altitude of 100 km. The visible panchromatic band, between 450 and 800 nm, is where the camera operates. The RC telescope used by OHRC is compact and has a long focus length. It records the signal and image onto a 12,000 pixel, 256 stage TDI detector. The TDI detector is necessary for signal gathering when there is little illumination and little time for integration. The detector can be changed using telecommands (TC) that let you choose the TDI stages and integration time. <Talk about the type of data given, and used for in this paper>

4. Denoising Diffusion Probabilistic Models

Diffusion models [x] are a type of probabilistic generative model that aims to learn the probability distribution of a dataset. They are based on the theory of non-equilibrium thermodynamics, which describes the behavior of systems that are not in thermodynamic equilibrium. The approach involves a gradual and systematic destruction of structure in a data distribution through an iterative forward diffusion process. That is followed by the learning of a reverse diffusion process that restores the structure in the data, this result in a highly flexible and a tractable generative model.

Let's provide a brief overview of the formulation of DDPMs [x]. This formulation incorporates several simplifying assumptions, one of which is a fixed noising process q that introduces diagonal Gaussian noise at each timestep.

4.1. Forward Diffusion

In forward diffusion process we gradually add Gaussian noise to a given data distribution $x_0 \sim q(x_0)$ over T discrete time steps. This process is defined as:

$$q(x_1, .., x_T \mid x_0) := \prod_{t=1}^{T} q(x_t \mid x_{t-1}) \quad (1)$$

$$q(x_t \mid x_{t-1}) := \mathcal{N}(x_t ; \sqrt{1 - \beta_t} x_{t-1}, \beta_t, \mathbf{I}) \quad (2)$$

where $\epsilon \sim \mathcal{N}(0, \mathbf{I})$ is the injected noise and $\beta_t \in (0, 1)$ controls the variance at each step t. This iteratively diffuses the data x_0 into latents x_1 through x_T by adding small amounts of Gaussian noise. We use a cosine schedule for setting the β_t values, with a slow noise rate early in the diffusion followed by accelerated noise near timestep T. With a sufficiently long diffusion horizon T and well-tuned schedule, the latent representation x_T approaches an isotropic Gaussian distribution that destroys the structure in x_0. The amount of noise added at each step is controlled by the β schedule, which requires careful tuning to balance destruction of original signal and training dynamics.

4.2. Reverse Diffusion

The forward diffusion process is reversed by training a model $p_\theta(x_t - 1|x_t)$ that predicts the less noised latent $x_t - 1$ from x_t at each discrete time step t. This trainable reverse process removes the added Gaussian noise to recover the original data x_0 from the isotropic latent x_T. The model pθ(xt-1|xt) is a neural network parameterized by θ that approximates the true conditional distribution $q(x_t - 1|x_t)$ at each timestep. By composing the reverse model over timesteps, we obtain a full generative distribution $p_\theta(x_{0:T})$ that can sample from the data space.

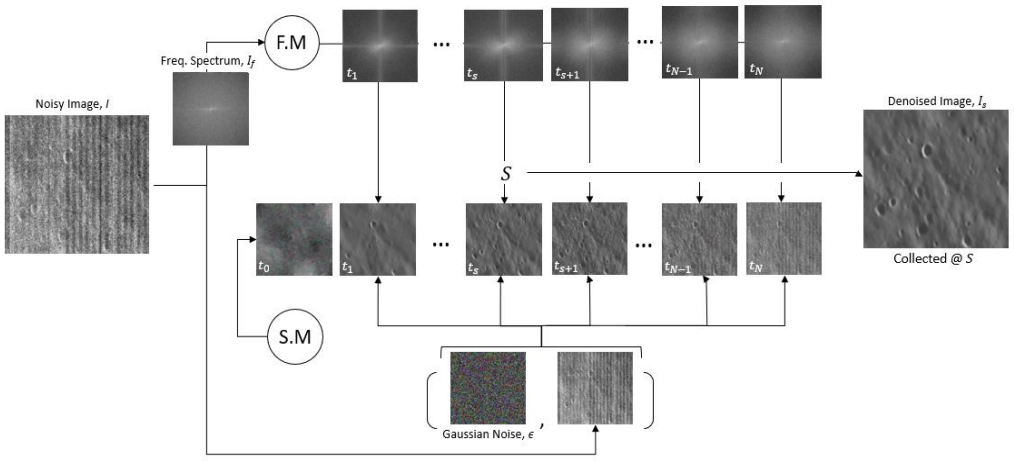

Figure 3: Denoising Workflow.

We define a prior $p_\theta(x_T) = \mathcal{N}(0, \mathbf{I})$ on the isotropic latent space. The reverse model p_θ is trained to maximize the log likelihood of the ground truth data x_0 under this full generative process. The neural network architecture for p_θ consists of a U-Net with skip connections between the encoder and decoder. This allows combining information at different scales to generate detailed samples. The reverse diffusion provides a way to regenerate data by gradually denoising the isotropic latent variable.

$$p_\theta^{(t)}(x_{t-1} \mid x_t) := \mathcal{N}(x_{t-1}\,;\, \mu_\theta(x_t, t), \sum_\theta(x_t, t)) \quad (3)$$

4.3. Optimization Procedure

Training the reverse diffusion model $p_\theta(x_t - 1|x_t)$ requires optimizing the variational lower bound (VLB) on the negative log-likelihood of the true data distribution. This encourages the learned generative distribution to match the real data. We approximate the intractable true posterior $q(x_t - 1|x_t)$ with our reverse model $p_\theta(x_t - 1|x_t)$ and optimize the evidence lower bound (ELBO) using stochastic gradient descent. The loss function is simplified to a noise prediction objective that trains p_θ to remove the diffused noise:

$$L_t := E_{t,x_0,\epsilon}\left[\left|\left|\epsilon - \epsilon_\theta(x_t, t)\right|\right|^2\right] \quad (4)$$

where $\epsilon_t \sim \mathcal{N}(0, \mathbf{I})$ is the injected noise at timestep t. This predicts the noise residual required to recover $x_t - 1$ from x_t. In addition to L_{simple}, we employ improved objective functions like L_{vip} [1] that weight noise predictions to focus more on early timesteps. The goal is to minimize the difference between the true posterior $q(x_t - 1|x_t)$ and our learned approximation $p_\theta(x_t - 1|x_t)$. This amounts to predicting the diffused noise as accurately as possible across timesteps. We validate convergence using log-likelihood and sample quality on a held-out set. The optimization enables efficiently learning the reverse generative process.

5. Experiments

5.1. Prior Training

The foundation of our unsupervised lunar image denoising workflow is a diffusion probabilistic model pretrained on sunlit lunar surface images. The model consists of two components - a spatial domain diffusion model trained on raw pixel values, and a concurrent frequency domain model trained on 2D Fourier transforms of the images. For model training, we utilize the sunlit-images from Chandrayaan-2's OHRC dataset, having a high spatial resolution of 0.25-0.30 m/pixel. This allows the model to learn fine-scale textural details. The spatial and frequency models are trained jointly on 256x256 images from the OHRC dataset using a U-Net architecture and variational inference objective. The spatial model learns localized relationships in lunar imagery while the frequency model encodes spectral correlations. During denoising, these priors guide the model to produce realistic reconstructions consistent with the training distribution.

5.1.1. Spatial Priors

A diffusion probabilistic model is trained on a dataset of 256x256 pixel images capturing 300 x 300-meter regions on the lunar surface under sunlit conditions. The model uses a U-Net architecture to learn a forward

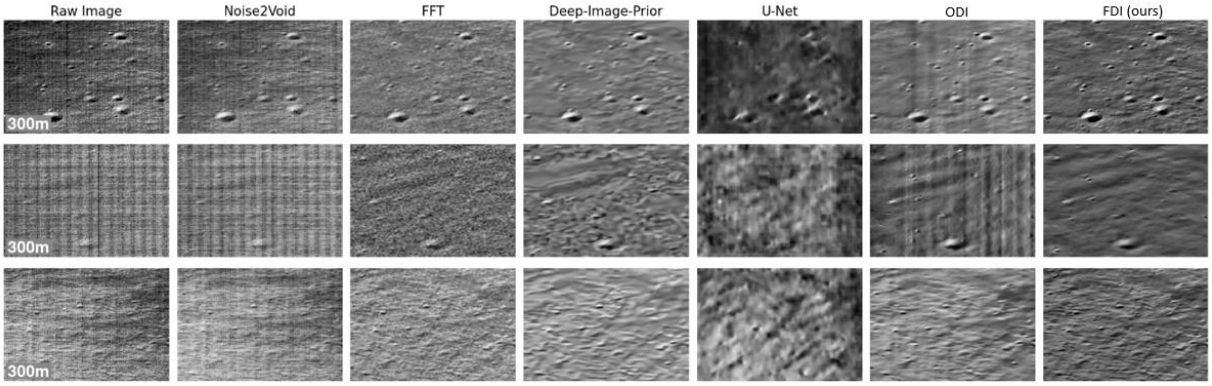

Figure 4: NAC cross-inference.

diffusion process that adds noise to images from the data distribution, as well as a reverse process to remove noise and generate high-fidelity lunar images. The forward process $q(x_t - 1|x_t)$ diffuses an image x_0 by adding small amounts of noise over T time steps, resulting in a noisy image x_T. The reverse process $p(x_t - 1|x_t)$ is trained to remove the diffused noise and recover the original image details. The model is trained by optimizing the variational lower bound on the log-likelihood, using L2 loss over 100 epochs with the Adam optimizer and learning rate of 1e-4. This allows the model to implicitly learn the spatial and textural statistics of lunar imagery in the latent space. Sampling from the reverse process generates new lunar images adhering to the spatial priors captured during training

5.1.2. Frequency Priors

In addition, with training the diffusion model on spatial lunar images, we also train a concurrent model on frequency domain representations of the data. The lunar images are transformed into the frequency domain using a 2D Discrete Fourier transform (DFT), yielding Fourier coefficients capturing the spectral composition. A separate diffusion model is trained on these frequency representations, following the same procedure as the spatial model. This frequency domain model learns generative priors over the Fourier coefficients that represent plausible lunar texture spectra. During sampling, we perform diffusion in both domains simultaneously - adding noise in frequency space and reversing the process to output lunar-like Fourier coefficients. These are converted back to the spatial domain using an inverse DFT, resulting in a lunar image guided by the learned frequency priors. This spectrally-conditioned result is then averaged with the output of the spatial model to incorporate multi-scale constraints. By modeling both spatial and frequency domains together, the generative process leverages complementary information. The frequency regularization serves as a spectral constraint to improve spatial consistency and texture details.

5.2. Modified Inference

We create an altered inference model in which we use the spatial and frequency models as priors. Firstly, we input a noisy sample, *I*, into the inference model, where we further split the input into spatial input, I_s, and its frequency counterpart, I_f. For every reverse diffusion step, we aim to use spatial priors to accelerate the lunar surface reconstruction in pixel-space relative to sensor noise. Simultaneously, I_f is also passed to an **Acceleration Unit** (AU), where we aim to perform additional accelerated reconstruction based on frequency correlations. Finally, we convert it back to physical space, and then average the guided images. Secondly, we combine white Gaussian noise (ϵ) at every time-step to diffuse the entire process. While performing *N* diffusion steps, we aim to simulate the sensor noising process by reconstructing the initial noisy image. Finally, we halt the process at an intermediate step, *S*, where the lunar surface reconstruction is almost complete, and noise reconstruction is just beginning. With this, we hope to sample guided denoised images resembling the input sunlit-image data distribution.

$$\hat{x}_t^{pre} := SM(x_t, t) + FM(x_t, t) \quad (5)$$

$$\hat{x_t} = y + \hat{x}_t^{pre} \quad (6)$$

$$x_t = A\,x_t + B\,\hat{x_t} + C\,\epsilon - \delta \quad (7)$$

$$x_t = x_t + \hat{x}_t^{pre} \quad (8)$$

Here, δ is and additional term which defines negative distribution shift of x_t.

5.3. Baselines

We compare our approach with the standard baselines in

Camera Type	N2V	FFT	Deep Image Prior	U-Net	ODI	FDI
	PSNR / SSIM / L1					
NAC	25.71 / 0.31 / 4.90	33.61 / 0.84 / 4.65	35.10 / 0.85 / 4.64	40.13 / 0.89 / 3.34	**41.84 / 0.93 / 1.45**	**44.39 / 0.96 / 1.21**
	KID					
OHRC	0.67	0.054	0.051	0.049	**0.01**	**0.003**

Table 1: OHRC/NAC metrics.

CH2-OHRC and LROC NAC separately.

NAC uses the **ISIS** calibration routine, while OHRC uses a separate **calibration correction coefficient** to remove the dark current offsets and then applies flatfield correction. These calibration routines are very primitive and don't yield any useful results.

Fast Fourier Transform (FFT). We manually create an FFT filtering algorithm to remove the vertical and horizontal strip-lines. We replace the DC-component (Zero frequency component) of the image with the average of its neighboring pixels. Lastly, we apply a Gaussian kernel with a standard deviation of 0.30 m-1.

Noise2Void (N2V). This is a self-supervised method, requiring training on only a single image. To denoise the PSR images, we pass the structure noise capture argument to denoise the sensor noise.

Deep Image Prior. Instead of using priors captured from pre-trained models, we use low-level priors obtained from a randomly initialized Deep CNN architecture on the fly with no prior training. We halt denoising halfway to prevent the sensor noise from propagating.

End-to-End U-Net. We train a standard U-Net architecture to predict Is from I directly in a supervised manner. A synthetic noise model, including Poisson noise, Gaussian noise, and vertical and horizontal stripes, is used to approximate the unknown noise profile.

Ordinary Diffusion Inference (ODI). Only the spatial priors are used for the denoising workflow, and the Acceleration Unit (AU) isn't included to reinforce the process with frequency priors.

6. Results

6.1. Filtered Diffusion Inference (FDI) Results

The filtered diffusion model achieved strong quantitative results on the test set. The high PSNR and SSIM scores indicate that the model is generating images very close to the ground truth, while the low L1 distance shows that pixel-wise errors are small. The joint model priors increase correlated spatial and frequency inference, significantly improving image quality over the baseline diffusion models by better preserving both high and low frequency details.

Qualitatively, the samples have sharp edges and fine details with no horizontal or vertical stripes, which can be attributed to dark current noise coupled with stochastic photon noise and minimal artifacts. This demonstrates the benefit of guidance from the spatial and frequency prior during image guidance and diffusion inferencing, facilitating a double-end acceleration of surface statistics relative to the noise. Additionally, the Kernel-Inception-Distance (KID) score for CH-2's OHRC samples are extremely low, indicating proximity to the sunlit-image data distribution.

6.2. ODI Results

The ordinary diffusion model achieved good but slightly inferior quantitative results compared to the filtered diffusion model. The gap in performance indicates that the spatial-only prior provides useful but insufficient guidance during sampling, leading to some degradation in image quality. In particular, the higher L1 distance and comparatively higher KID score for CH-2's OHRC test samples suggest that the samples have slightly more pixel-wise error and show a prominent deviation from the desired levels.

Qualitatively, while samples are realistic, some fine details are oversmoothed, and edges are not as sharp. More importantly, due to the absence of spectral guiding, the strip-noises are still present during inferencing, resulting in lower comparative acceleration. Still, the spatial prior alone produces respectable results.

6.3. End-to-End U-Net Results

The end-to-end U-Net model achieved lower quantitative scores compared to the previous two models. The synthetic noise model provides a useful training signal but is insufficient to reach the level of performance achieved by diffusion probabilistic modeling. Without a high-quality noise model, the model struggles to generate high-fidelity details, which is reflected in the lower PSNR and SSIM scores. This is because the entire training pipeline depends on the quality of the noise model. The model is unable to approximate the noise profile, especially when cross-inferred on LRO's NAC PSR image samples. The higher L1 score also indicates greater pixel-level deviation from the ground truth images.

Qualitatively, the samples are blurrier and lack well-defined details compared to the diffusion models. This

demonstrates the benefits of iterative refinement during sampling for image generation. The end-to-end approach may be reasonable for learning broad contours but lacks a robust probabilistic framework for realistic synthesis.

7. Conclusion and Future Works

We have presented an unsupervised approach for image denoising in extreme low-light scenarios in the lunar poles. Our work is novel in several aspects; we are the first to present an unsupervised denoising method in this setting to work with extremely constrained data availability in using CH-2's OHRC image dataset. We also show that due to our training dependence on high resolution sunlit-image dataset we can perform out-of-distribution inference in denoising on LRO NAC's PSR image dataset, despite it having much different and more complex sensor noise distribution. Our qualitative and quantitative results showed that our method strongly outperforms common calibration baselines and other unsupervised denoising baselines, and also compares with the state-of-the-art supervised method in this domain.

Our future work will involve a quantitative assessment of this method through the use of downstream tasks on real images, including crater counting and elevation modeling. We will also explore further improvements in our training image scene selection, with a focus on tailoring it to specific tasks. For instance, we will investigate the training of our networks to capture image transition zones between PSRs and sunlit regions, which holds particular relevance for upcoming exploration missions.

References

[1] Roy Chowdhury, Arup & Patel, Vishnu & Joshi, Satya & Arya, Ashutosh & Kumar, Ankush & Paul, Sukamal & Shah, Dhrupesh & Soni, Pradeep & Karelia, J & Sampat, Minal & Sharma, Satish & Somani, Sandeep & Bhagat, Virendra & Sharma, Jitendra & Amitabh, & K., Suresh & Rajashekhar, & Bokarwadia, B & Kumar, Mukesh & Ghonia, D. (2020). Terrain Mapping Camera-2 onboard Chandrayaan-2 Orbiter. Current Science. 118. 566. 10.18520/cs/v118/i4/566-572.

[2] Bussey, D. & McGovern, J. & Greenhagen, B. & Paige, D. & Cahill, J. & Siegler, Matthew & Spudis, P.. (2012). Global Catalogue of Lunar Permanently Shadowed Regions. Meteoritics and Planetary Science Supplement.

[3] Sohl-Dickstein, Jascha, et al. "Deep unsupervised learning using nonequilibrium thermodynamics." International Conference on Machine Learning. PMLR, 2015.

[4] Roy Chowdhury, Arup & Banerjee, Arup & Joshi, Satya & Dutta, Moumita & Kumar, Ankush & Bhattacharya, Satadru & Rehman, Sami & Bhati, Sunil & Karelia, J & Biswas, Amiya & Saxena, Anish & Sharma, Satish & Somani, Sandip & Bhagat, Virendra & Sharma, Jitendra & Ghonia, D & Bokarwadia, B & Prashar, Ajay. (2020). Imaging Infrared Spectrometer onboard Chandrayaan-2 Orbiter. Current Science. 118. 368-375. 10.18520/cs/v118/i3/368-375.

[5] Bhiravarasu, Sriram S., et al. "Chandrayaan-2 dual-frequency synthetic aperture radar (DFSAR): Performance characterization and initial results." The Planetary Science Journal 2.4 (2021): 134.

[6] Roy Chowdhury, Arup & Saxena, Manish & Kumar, Ankush & Joshi, Satya & Amitabh, & Dagar, Aditya & Mittal, Manish & Kirkire, Shweta & Desai, Jalshri & Shah, Dhrupesh & Karelia, J & Anand, Kumar & Jha, Kailash & Das, Prasanth & Bhagat, Virendra & Sharma, Jitendra & Ghonia, D & Desai, Meghal & Bansal, Gaurav & Gupta, Ashutosh. (2020). Orbiter High Resolution Camera onboard Chandrayaan-2 Orbiter. Current Science. 118. 560. 10.18520/cs/v118/i4/560-565.

[7] Ho, Jonathan, Ajay Jain, and Pieter Abbeel. "Denoising diffusion probabilistic models." Advances in Neural Information Processing Systems 33 (2020): 6840-6851.

[8] Li, Chongyi, Chunle Guo, and Chen Change Loy. "Learning to enhance low-light image via zero-reference deep curve estimation." IEEE Transactions on Pattern Analysis and Machine Intelligence 44.8 (2021): 4225-4238.

[9] B. Moseley, V. Bickel, I. G. López-Francos and L. Rana, "Extreme Low-Light Environment-Driven Image Denoising over Permanently Shadowed Lunar Regions with a Physical Noise Model," 2021 IEEE/CVF Conference on Computer Vision and Pattern Recognition (CVPR), Nashville, TN, USA, 2021, pp. 6313-6323, doi: 10.1109/CVPR46437.2021.00625.

[10] Bickel, V.T., Moseley, B., Lopez-Francos, I. et al. Peering into lunar permanently shadowed regions with deep learning. Nat Commun 12, 5607 (2021). https://doi.org/10.1038/s41467-021-25882-z

[11] Abirami R. Nandhini, Vincent P. M. Durai Raj, Low-Light Image Enhancement Based on Generative Adversarial Network, Frontiers in Genetics, 2021.

[12] Van den Oord, Aaron, et al. "Conditional image generation with pixelcnn decoders." Advances in neural information processing systems 29 (2016).

[13] Lehtinen, Jaakko, et al. "Noise2Noise: Learning image restoration without clean data." arXiv preprint arXiv:1803.04189 (2018).

[14] Krull, Alexander, Tim-Oliver Buchholz, and Florian Jug. "Noise2void-learning denoising from single noisy images." Proceedings of the IEEE/CVF conference on computer vision and pattern recognition. 2019.

[15] Prakash, Mangal, Alexander Krull, and Florian Jug. "Fully unsupervised diversity denoising with convolutional variational autoencoders." arXiv preprint arXiv:2006.06072 (2020).

[16] Prakash, Mangal, et al. "Interpretable unsupervised diversity denoising and artefact removal." arXiv preprint arXiv:2104.01374 (2021).

[17] Salmon, B., Krull, A. (2023). Towards Structured Noise Models for Unsupervised Denoising. In: Karlinsky, L., Michaeli, T., Nishino, K. (eds) Computer Vision – ECCV 2022 Workshops. ECCV 2022. Lecture Notes in Computer Science, vol 13804. Springer, Cham.

[18] H. D. Cheng and X. J. Shi. A simple and effective histogram equalization approach to image enhancement. Digital Signal Processing: A Review Journal, 14(2):158–170, 2004

[19] Ronneberger, Olaf, Philipp Fischer, and Thomas Brox. "U-net: Convolutional networks for biomedical image

segmentation." Medical Image Computing and Computer-Assisted Intervention–MICCAI 2015: 18th International Conference, Munich, Germany, October 5-9, 2015, Proceedings, Part III 18. Springer International Publishing, 2015.

[20] Emerson J. Speyerer, Mark S. Robinson, Persistently illuminated regions at the lunar poles: Ideal sites for future exploration, Icarus, Volume 222, Issue 1, 2013, Pages 122-136, ISSN 0019-1035, https://doi.org/10.1016/j.icarus.2012.10.010.

[21] Betzalel, Eyal, et al. "A Study on the Evaluation of Generative Models." arXiv preprint arXiv:2206.10935 (2022).